Monthly Notices
of the
ROYAL ASTRONOMICAL SOCIETY

MNRAS **495,** 1461–1467 (2020)
Advance Access publication 2020 May 13

doi:10.1093/mnras/staa1310

Optical spectroscopy and X-ray observations of the D-type symbiotic star EF Aql

K. A. Stoyanov,[1]★ K. Iłkiewicz,[2] G. J. M. Luna,[3,4,5] J. Mikołajewska,[2] K. Mukai,[6,7] J. Martí,[8] G. Latev,[1] S. Boeva[1] and R. K. Zamanov[1]

[1]*Institute of Astronomy and National Astronomical Observatory, Bulgarian Academy of Sciences, Tsarigradsko Chaussee 72, BG-1784 Sofia, Bulgaria*
[2]*Nicolaus Copernicus Astronomical Centre, Polish Academy of Sciences, Bartycka 18, PL-00716 Warsaw, Poland*
[3]*Instituto de Astronomía y Física del Espacio (IAFE), CONICET-Universidad de Buenos Aires, Av. Inte. Güiraldes 2620, C1428ZAA Buenos Aires, Argentina*
[4]*Facultad de Ciencias Exactas y Naturales, Universidad de Buenos Aires, C1428EGA Buenos Aires, Argentina*
[5]*Universidad Nacional de Hurlingham, Av. Gdor. Vergara 2222, Villa Tesei, 1686 Buenos Aires, Argentina*
[6]*CRESST and X-ray Astrophysics Laboratory, NASA Goddard Space Flight Center, Greenbelt, MD 20771, USA*
[7]*Department of Physics, University of Maryland, Baltimore County, 1000 Hilltop Circle, Baltimore, MD 21250, USA*
[8]*Departamento de Física (EPSJ), Universidad de Jaén, Campus Las Lagunillas A3-420, E-23071 Jaén, Spain*

Accepted 2020 May 5. Received 2020 May 5; in original form 2020 February 13

ABSTRACT

We performed high-resolution optical spectroscopy and X-ray observations of the recently identified Mira-type symbiotic star EF Aql. Based on high-resolution optical spectroscopy obtained with the Southern African Large Telescope (SALT), we determine the temperature (∼55 000 K) and the luminosity (∼5.3 $L_{\odot}$) of the hot component in the system. The heliocentric radial velocities of the emission lines in the spectra reveal possible stratification of the chemical elements. We also estimate the mass-loss rate of the Mira donor star. Our *Swift* observation did not detect EF Aql in X-rays. The upper limit of the X-ray observations is 10^{-12} erg cm^{-2} s^{-1}, which means that EF Aql is consistent with the faintest X-ray systems detected so far. Otherwise we detected it with the UltraViolet and Optical Telescope (UVOT) instrument with an average *UVM2* magnitude of 14.05. During the exposure, EF Aql became approximately 0.2 *UVM2* magnitudes fainter. The periodogram analysis of the *V*-band data reveals an improved period of 320.4 ± 0.3 d caused by the pulsations of the Mira-type donor star.

Key words: accretion, accretion discs – stars: AGB and post-AGB – binaries: symbiotic – stars: individual: EF Aql.

1 INTRODUCTION

EF Aquilae (EF Aql) was identified as a variable star on photographic plates from Königstuhl Observatory (Reinmuth 1925). Richwine et al. (2005) have examined the optical photometry for EF Aql and classify it as a Mira-type variable with a period of 329.4 d and amplitude of variability >2.4 mag in *V* band. Margon et al. (2016) reported that it has bright ultraviolet (UV) flux, prominent Balmer emission lines, and [O III] λ5007 emission. Thus EF Aql is classified as a symbiotic star, belonging to the symbiotic Mira subgroup. Zamanov et al. (2017) showed that EF Aql displays flickering (stochastic variability with amplitude ∼0.2 mag on a time-scale of ∼20 min) in *B* and *V* bands, which is a rarely detectable phenomenon among the symbiotic stars (Sokoloski, Bildsten & Ho 2001).

Symbiotic stars are long-period interacting binaries, consisting of a yellow or red giant transferring mass to a hot compact object. According to the classification of Webster & Allen (1975), the symbiotic stars are divided into two types – those with cool stellar continuum (S-type) and those with infrared excess from dust (D-type). The D-type symbiotics have near-infrared (IR) variations that are caused by the presence of a thermally pulsating Mira-type variable, while in S-type symbiotic stars a normal red giant is present. Allen (1982) introduced D'-type symbiotic stars, in which dust is present and a cool giant of spectral type F or G is the donor. The orbital periods of the symbiotic stars are in the range of 100 d to more than 100 yr (Gromadzki, Mikołajewska & Soszyński 2013). The D-type symbiotics have longer orbital periods (Hinkle et al. 2013), because the orbits need to be wide enough to harbour a Mira variable with a diameter of several astronomical unit (au) and a mass of ∼1–3 $M_{\odot}$ (Vassiliadis & Wood 1993). In most symbiotic stars, the secondary is a hot and luminous accreting white dwarf (Mikołajewska 2012). In a few cases has the secondary been shown to be a neutron star (Davidsen, Malina & Bowyer 1977; Kuranov & Postnov 2015). The whole symbiotic system is surrounded by a circumstellar nebula formed by the matter lost from the components.

★ E-mail: kstoyanov@astro.bas.bg

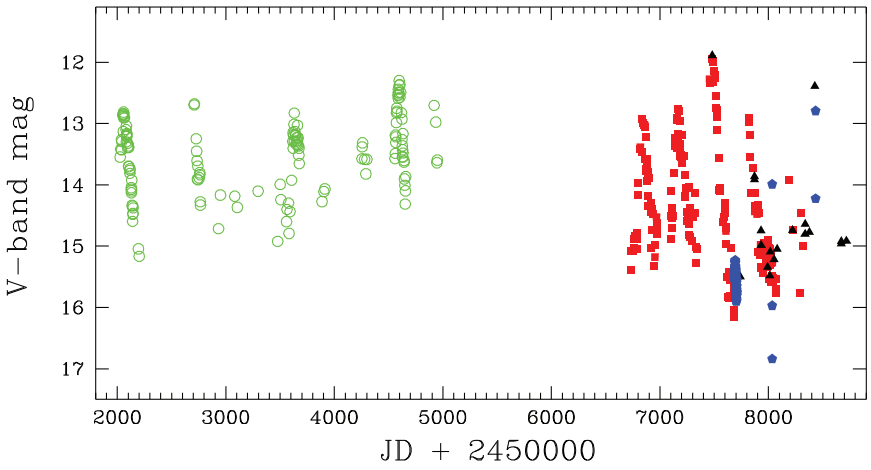

Figure 1. The *V*-band photometric observations of EF Aql. The green open circles represent the data from ASAS; the red squares represent the data from ASAS-SN; the blue pentagons represent the data from AAVSO; and the black triangles are the observations from Rozhen National Astronomical Observatory.

Table 1. $UBVR_CI_C$ photometry of EF Aql obtained on 2019 July 6.

Date	Band	Magnitude
2019-07-06 01:49	*U*	14.46 ± 0.08
2019-07-06 01:52	*B*	15.41 ± 0.06
2019-07-06 01:56	*B*	15.53 ± 0.07
2019-07-06 01:58	*V*	14.92 ± 0.06
2019-07-06 01:59	*V*	14.96 ± 0.05
2019-07-06 01:55	*R*	14.06 ± 0.03
2019-07-06 02:00	*R*	13.97 ± 0.03
2019-07-06 01:56	*I*	11.25 ± 0.03
2019-07-06 02:00	*I*	11.28 ± 0.03

2 OBSERVATIONS

2.1 Photometry

The *V*-band light curve of EF Aql based on data from the All-Sky Automated Survey (ASAS; Pojmanski 1997), All-Sky Automated Survey for Supernovae (ASAS-SN; Shappee et al. 2014; Kochanek et al. 2017), and American Association of Variable Star Observers (AAVSO) International Database is shown in Fig. 1. In addition, a $UBVR_CI_C$ photometric series of EF Aql was obtained in the period 2016–2019 with the 50/70-cm Schmidt telescope of the Rozhen National Astronomical Observatory, Bulgaria. Journal of $UBVR_CI_C$ observations, obtained on 2019 July 6, is given in Table 1.

2.2 SALT observations

Spectroscopic observations were carried out on 2019 June 7, 2019 July 9, and 2019 July 14 with the 11-m Southern African Large Telescope (SALT; Buckley, Swart & Meiring 2006; O'Donoghue et al. 2006) using the High Resolution Spectrograph (HRS; Bramall et al. 2010, 2012; Crause et al. 2014). The time of observations corresponds to phases $\Phi = 0.61$, 0.71, and 0.72, respectively (for details see Section 3.1). The exposure times are 1900 s. The spectrograph was used in a medium-resolution mode with resolving power $R \sim 40\,000$ and wavelength coverage of 4000–8800 Å. The initial data reduction was performed using PySALT pipeline (Crawford et al. 2010) that was followed by HRS pipeline (Kniazev, Gvaramadze & Berdnikov 2017), based on MIDAS FEROS (Stahl, Kaufer & Tubbesing 1999) and ECHELLE (Ballester 1992) packages. In Table 2, we present the measured equivalent widths (EWs), full widths at half-maximum (FWHMs), and heliocentric radial velocities (RV_{hel}) of some emission lines in the spectrum of EF Aql. The measurements are done by employing a Gaussian fit. Figs 2 and 3 show the regions around the Hα and Hβ emission lines.

2.3 *Swift* observations

X-ray and UV observations were obtained using the *Neil Gehrels Swift Observatory* (hereafter *Swift*) on 2019 September 12 (ObsID: 00011552001). The X-Ray Telescope (XRT) was operated in photon-counting mode, while the UltraViolet and Optical Telescope (UVOT) was operated in imaging mode using *UVM2* filter, centred approximately at 2200 Å, and both achieved a total exposure of approximately 3.8 ks.

3 RESULTS

3.1 Period of pulsations

Using the photometric data, we performed periodogram analysis in order to confirm and improve the detected period of 329.4 d that is associated with the pulsations of the Mira-type donor star (Richwine et al. 2005). Using the CLEAN algorithm (Roberts, Lehar & Dreher 1987), phase dispersion minimization (PDM) method (Stellingwerf 1978), and Fourier transform, we obtained periods of 321.2 ± 0.1, 320.8 ± 0.1, and 320.4 ± 0.3 d, respectively. We present the periodograms of the CLEAN and PDM methods in Fig. 4. The period and the amplitude of the pulsations (∼4 mag, see Fig. 1) are typical for the Mira-type variables (Whitelock et al. 2003). For the purposes of our study, we use the following ephemeris:

$$\mathrm{JD_{max}} = (245\,8127.3 \pm 1.6) + (320.4) \pm 0.3 \times E. \quad (1)$$

We present the *V*-band light curve of EF Aql folded with the period of 320.4 d in Fig. 5.

3.2 Distance and interstellar reddening

As Le Bertre et al. (2003) classified EF Aql as an O-rich star, we could use the period–luminosity relations for Miras for estimation of the distance to the object (Whitelock, Feast & Van Leeuwen

Table 2. The measured equivalent widths (EWs), full widths at half-maximum (FWHMs), and heliocentric velocities of the lines in the spectrum of EF Aql. Negative values of EWs denote emission lines, while positive values denote absorption lines.

Line	2019-06-07			2019-07-09			2019-07-14		
	EW (Å)	FWHM (km s^{-1})	RV_{hel} (km s^{-1})	EW (Å)	FWHM (km s^{-1})	RV_{hel} (km s^{-1})	EW (Å)	FWHM (km s^{-1})	RV_{hel} (km s^{-1})
Hα 6562.82	− 88.40	83	3.4	− 90.7	74	2.8	− 88.8	74	1.0
Hβ 4861.33	− 11.37	85	0.8	− 10.4	60	− 0.8	− 11.4	59	− 3.1
Hγ 4340.47	− 2.78	58	− 2.1	− 1.51	44	− 3.7	− 3.27	44	− 3.2
He I 4471.48	− 1.46	63	7.9	− 1.34	71	− 2.1	–	–	–
He I 4713.14	− 0.1	38	12.3	− 0.06	37	3.5	− 0.08	15	− 0.8
He I 4921.93	− 1.33	91	16.2	− 2.92	152	17	− 3.80	120	15.9
He I 5015.68	− 2.57	115	19.3	− 3.72	132	12	− 5.94	130	21
He I 5875.64	− 3.19	67	2.4	− 3.31	53	− 11.9	− 2.07	39	− 2.9
He I 6678.15	− 0.95	48	6.3	− 0.30	28	− 2.5	− 0.50	33	− 2.1
He I 7065.19	− 1.66	52	1.5	− 0.90	32	− 0.8	− 1.40	35	− 1.4
[O III] 4363.21	− 0.37	41	− 6.3	− 0.39	34	− 7.8	− 0.52	32	− 6.0
[O III] 4958.92	− 0.75	25	− 12.2	− 0.99	27	− 10.9	− 1.29	25	− 12.0
[O III] 5006.85	− 1.66	25	− 11.9	− 1.57	26	− 12.0	− 2.56	28	− 12.5
[O I] 8446.60	− 2.69	60	2.2	–	–	–	− 1.32	42	− 2.3
Fe II 38 4549.47	− 0.92	63	− 0.5	− 0.24	36	3.4	–	–	–
Fe II 38 4583.83	− 0.71	52	4.9	− 0.58	50	0.8	− 0.54	49	7.0
Fe II 37 4629.34	− 0.82	90	6.9	− 0.58	110	17.2	− 0.89	67	3.7
Fe II 42 4923.92	− 1.95	79	3.4	− 1.18	64	12.7	− 2.68	88	8.6
Fe II 42 5018.43	− 1.84	67	4.9	− 1.92	74	8.4	− 2.61	69	7.3
[N II] 6583.29	− 0.41	38	− 11.2	− 0.31	34	− 13.7	− 0.27	27	− 5.4
Na I D1 5889.95	0.45	19	− 15.8	0.31	14	− 16.7	0.33	16	− 12.8
Na I D2 5895.92	–	–	–	0.29	15	− 16.4	0.24	13	− 13.0

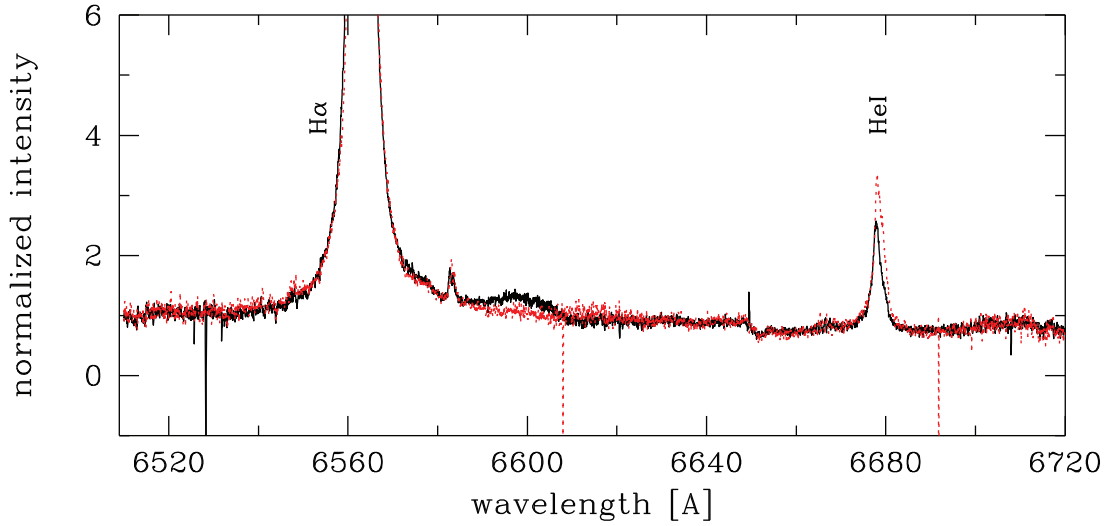

Figure 2. The region around Hα in the spectrum of EF Aql. Black solid line is for 2019 June 7 observation and red dashed line is for 2019 July 14 observation.

2008):

$$M_K = \rho[\log P - 2.38] + \delta, \quad (2)$$

where $\rho = -3.51 \pm 0.20$ and $\delta = -7.25 \pm 0.07$ (Gromadzki et al. 2009). We derive mean K-band magnitude from the Two Micron All-Sky Survey (2MASS) All Sky Catalog and DENIS data base, $K = 4.78 \pm 0.58$, and absolute K-band magnitude, $M_K = -7.69$, obtained using equation (2). In Zamanov et al. (2017), we assumed interstellar extinction $E(B-V) = 0.45$, which seems much overestimated. The NASA/IPAC Infrared Science Archive (IRSA; Galactic Reddening and Extinction Calculator) gives low extinction through the Galaxy in the direction of EF Aql, $E(B-V) < 0.17$, so the extinction in K band should be insignificant. From these magnitudes we estimate the distance to EF Aql to be $d = 3.1$ kpc.

In order to estimate the interstellar plus circumstellar extinction, we compare the observed and intrinsic $J-K$ colours. Using the period–colour relation by Whitelock, Marang & Feast (2000) for O-rich Miras:

$$(J-K)_0 = 0.71 \log P - 0.39. \quad (3)$$

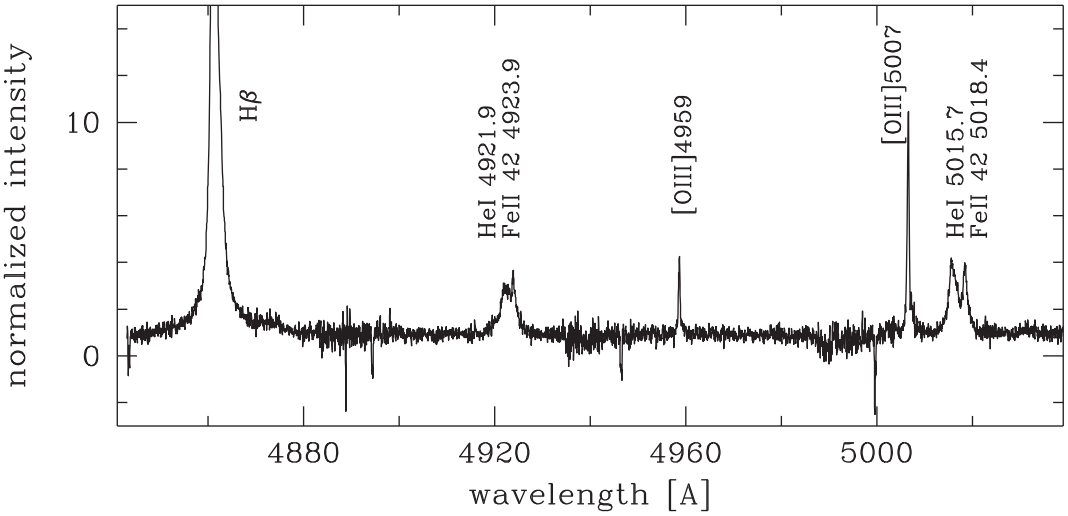

Figure 3. The emission lines around the Hβ line in the spectrum of EF Aql.

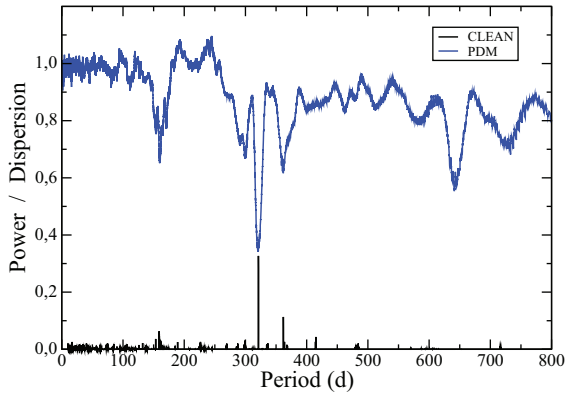

Figure 4. Periodograms for the *V*-band magnitude of EF Aql computed using the CLEAN and PDM algorithms. The period of pulsations of the Mira is detected as the most significant one.

The 2MASS All Sky Catalog and DENIS data base give observed $J - K$ colours 1.61 and 1.81, respectively, which corresponds to $E(J - K) = 0.32 \pm 0.10$.

In our spectra we do not detect DIB 6613 Å. No interstellar component is visible in K I 7699 line (see Fig. 6). The Na I D lines show complex profiles with a moderately broad emission and at least two narrow absorption components. The stronger blue absorption component may be of local origin, e.g. circumstellar material, while the red component is of interstellar origin. The EW of the Na D1 line is in the range 0.31–0.45 Å that corresponds to $E(B - V) = 0.12$–0.25 (Munari & Zwitter 1997). It is possible that $E(J - K)$ represents the total (circumstellar and interstellar) extinction and $E(B - V)$ marks only the interstellar extinction. This would indicate significant circumstellar reddening, as expected for a D-type symbiotic systems (Gromadzki et al. 2009).

3.3 Temperature and luminosity of the hot component

The minimum temperature is set by the maximum ionization potential observed in the spectrum that in our case is 35.12 eV corresponding to the [O III] lines (Peterson 1997). This gives a temperature $T_{\rm hot} \gtrsim 35\,000$ K. The lack of any traces of He II lines and the presence of strong He I lines means that $T_{\rm hot} \lesssim 60\,000$ K.

Using the photometric observations listed in Table 1, we estimate

$$F_{\rm cont}(R) \sim F_{\rm cont}(6580\,\text{Å}) \sim 5.6 \times 10^{-15}\,\text{erg s}^{-1}\,\text{cm}^{-2}. \quad (4)$$

This in combination with the measured EW of the Hα line (see Table 2) gives total flux in the Hα line,

$$F(\text{H}\alpha) \sim 9 \times 10^{-13}\,\text{erg s}^{-1}\,\text{cm}^{-2}.$$

Following the same pattern for the *V*-band magnitude and the He I 5876 Å line, and the *B*-band magnitude and the Hβ lines, the total fluxes in the lines are

$$F(\text{He I}\,5876) \sim 4 \times 10^{-14}\,\text{erg s}^{-1}\,\text{cm}^{-2},$$
$$F(\text{H}\beta) \sim 1.2 \times 10^{-13}\,\text{erg s}^{-1}\,\text{cm}^{-2}.$$

Assuming photoionization, case B recombination (Netzer 1975), and blackbody ionizing source/hot component, the ratio F(He I 5876)/F(Hβ) indicates $T_{\rm hot} \sim 55\,000$ K, and the total Hβ and He I 5876 fluxes imply a hot component luminosity $L_{\rm hot} \sim 5.3\,L_\odot$ using $d = 3.1$ kpc.

3.4 Mass-loss rate

The Mira pulsations play a crucial role in the mass-loss process because they raise the dense material from the atmosphere to distances where the temperature is too low to form dust grains. This is not a well-understood process in the case of the O-rich Miras. It is believed that a combination of the stellar pulsation and radiation pressure on dust is not enough to drive the mass loss (Woitke 2006) and the proper mechanism is a subject of debates.

To estimate the mass loss for EF Aql, we use the correlation between the mass-loss rate and the $K - [12]$ colour for O-rich Mira variables. The *K* and [12] fluxes originate from the star and the dust shell, respectively, so larger $K - [12]$ colour means thicker shell. Therefore, the $K - [12]$ colour provides a useful tool for mass-loss rate estimation. Using the mean *K*-band magnitude (see Section 3.2) and the flux at 12 μm provided by the *Infrared Astronomical Satellite* (*IRAS*) data base (Neugebauer et al. 1984), we estimate $K - [12] = 2.89$. Using fig. 21 from Whitelock et al. (1994), we estimate the mass-loss rate for EF Aql to be $\sim 2.5 \times 10^{-7}\,M_\odot\,\text{yr}^{-1}$. The mass-loss rates of the single O-rich Miras are in the range from 10^{-7} to $10^{-5}\,M_\odot\,\text{yr}^{-1}$ (Whitelock et al. 1994). The Miras in the symbiotic

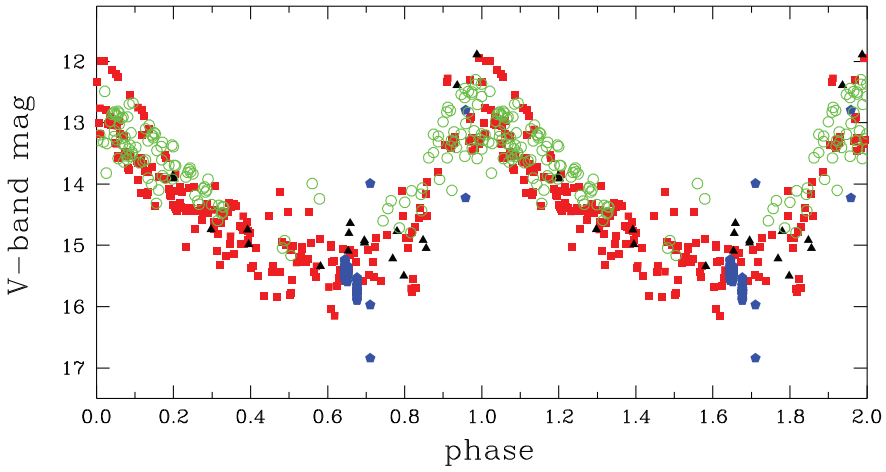

Figure 5. The *V*-band photometric observations of EF Aql folded with the period of the pulsations. The symbols are the same as in Fig. 1.

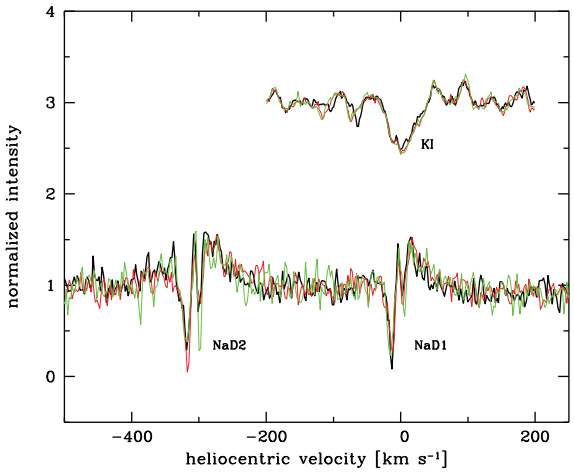

Figure 6. The spectra of EF Aql in Na D1 and K I 7699 lines. Black solid line is for 2019 June 7 obsevation, red dashed line is for 2019 July 9 observation, and green is for 2019 July 14 observation. Sharp interstellar absorptions are visible in Na D1 and Na D2 lines. No interstellar component is visible in K I 7699.

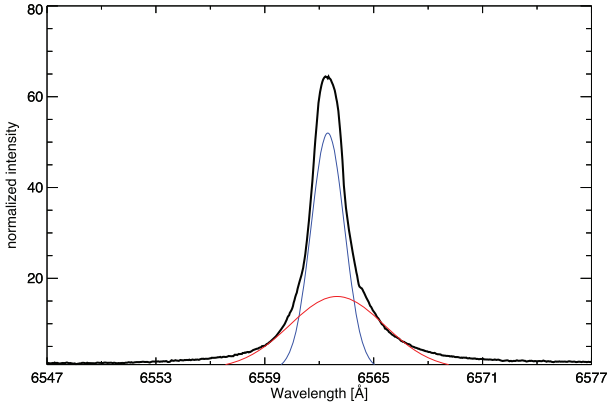

Figure 7. The broad and narrow components of the Hα line fitted with two Gaussians with full widths at half-maximum (FWHMs) $\sim$ 1.8 and 6.0 Å, respectively.

systems have an average mass-loss rate $\sim 3.2 \times 10^{-6}$ $M_\odot$ yr^{-1} (Gromadzki et al. 2009). The measured low value for EF Aql is in agreement with our considerations for a low-luminosity system (see the Discussion section).

3.5 X-ray and UV emission

Our *Swift* observation did not detect EF Aql in X-rays, with an upper limit of 0.003 counts s^{-1}. Assuming an absorbing column of 10^{23} cm^{-2} and a plasma temperature of 10 keV (typical of δ component in symbiotics), this upper limit on the count rate translates into an unabsorbed flux of 10^{-12} erg cm^{-2} s^{-1} and into a luminosity of about half a solar luminosity. This upper limit is consistent with the faintest δ components detected so far (the component from the boundary layer between the accretion disc and the white dwarf; Luna et al. 2013). In turn, we detected EF Aql with the UVOT instrument on-board *Swift*, with an average *UVM2* magnitude of 14.05 (uncorrected for reddening). During the 25 ks that *Swift* was pointing to EF Aql, we observed that it got approximately 0.2 *UVM2* magnitudes fainter. We can only speculate about this behaviour, which could be due to variable absorption and/or flickering from the accretion disc.

4 DISCUSSION

The Balmer lines show complex profiles with a relatively broad and a narrow component (Fig. 7). The same structure is present in the strongest He I lines (4471, 4713, 5876, 6678, and 7065 Å), while it is less obvious in the fainter lines. In the case of He I 4922 and He I 5016 the nearby Fe II lines may hide the fine structure of the He I lines (Fig. 3). No He II lines are detected in the spectra.

The [N II] 6583 line seems to have double-peaked structure with the red component 50–60 per cent of the blue one (Fig. 8) The same profile appears on all spectra. In the case of [O III] lines, only the blue component is visible. The line profile is very similar to that in planetary nebulae (Lutz et al. 1989) and it may be originate in a faint fossil nebula ejected by the present white dwarf component during its asymptotic giant branch (AGB) stage (Munari & Patat 1993).

It is also interesting that the Hα profile appears to have flat top, and, in principle, the narrow component may consist of two narrow lines with velocity separation similar to that found in [N II] profiles.

The temperature of the hot components in symbiotics is in the range 35 000–500 000 K and the luminosity is in the range

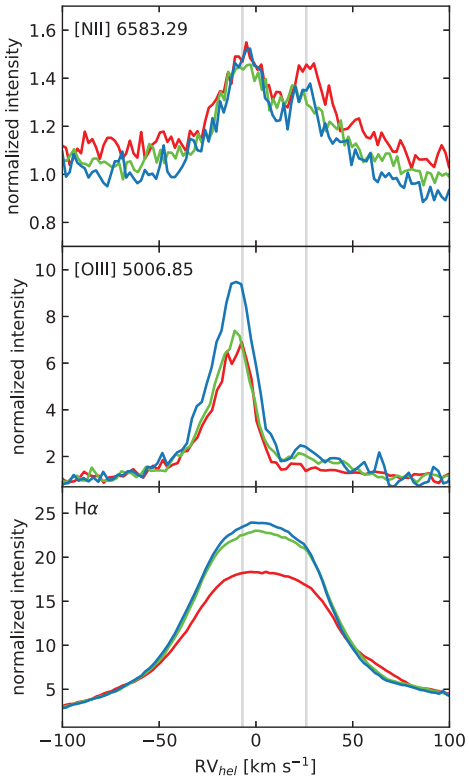

Figure 8. Comparison of emission lines profiles of EF Aql. The grey lines indicate the positions of two maxima in the [N II] 6583.29 line. Red line: SALT 2019 June 6 spectrum; green line: SALT 2019 July 9 spectrum; and blue line: SALT 2019 July 14 spectrum.

0.3–37 000 $L_\odot$ (Muerset et al. 1991; Murset & Nussbaumer 1994; Mikolajewska, Acker & Stenholm 1997; Orio et al. 2007). Mikolajewska et al. (1997) found that the temperature of the hot component correlates with the Raman scattered λ6825 line. The 6825 Å emission is produced due to Raman scattering of O VI λ1032 by hydrogen atoms (Schmid 1989). The lack of λ6825 emission in EF Aql supports our result for a hot component with low luminosity.

The typical red giant in symbiotic system has a mass-loss rate of $\sim 10^{-7}$ $M_\odot$ yr^{-1}, which is enough to power a luminosity of 10–100 $L_\odot$. In systems with hydrogen shell burning on the surface of the white dwarf, even an accretion rate of $\sim 10^{-8}$ $M_\odot$ yr^{-1} can produce that amount of luminosity. The Mira-type variables have a mass-loss rate of $\sim 10^{-5}$– 10^{-7} $M_\odot$ yr^{-1} (Whitelock et al. 1994), but the larger distance between the components in the D-type symbiotic stars results similar luminosities. In the systems without hydrogen shell burning on the surface of the white dwarf (the case of EF Aql), the luminosity of the hot component is more or less equal to that generated by the accretion (Paczynski & Zytkow 1978).

The obtained parameters set up EF Aql among the systems with lowest temperature and luminosity of the hot component and the most probable reason is the low accretion rate.

The AGB stage is the final stage of the evolution of the low- and intermediate-mass stars before they turn into white dwarfs. The evolution during this stage is driven by a large range of complex processes, including the stellar pulsations and the mass loss. The AGB stars can reach mass-loss rates so high that mass-loss process can determines the evolutionary time-scales, instead of nuclear burning time-scale. Large-scale convective flows bring newly formed chemical elements from the stellar interior to the surface and, boost by the stellar pulsations, they trigger shock waves in the extended stellar atmosphere, where they formed massive outflows of gas and dust. These outflows not only enrich the interstellar medium (ISM), but also play a crucial role in the evolution of the cool giant into a white dwarf (Höfner & Olofsson 2018). The progenitors of the short-period Miras have a mass of 1.0–1.1 $M_\odot$ (Jura 1994), while the Miras with periods in the range 400–600 d have progenitors with masses $\geq$2 $M_\odot$. The lifetime of a star with initial mass 1–2 $M_\odot$ during the AGB stage is in the range 1–3 $\times$ 10^6 yr (Kalirai, Marigo & Tremblay 2014). For a Mira with period $\sim$300 d, we should expect an increase of the period and the mass loss (Trabucchi et al. 2019). Following these considerations, for the future evolution of EF Aql we are expecting an increase of the accretion rate on to the white dwarf followed by an increase of the X-ray activity but the evolution of EF Aql in general should be consider in terms of the binary evolution.

EF Aql appears to be powered by accretion on to a white dwarf without shell nuclear burning on the surface of the white dwarf. The presence of optical flickering (Zamanov et al. 2017) and the modest hot component luminosity (this work) are both consistent with this interpretation. While we did not detect EF Aql in X-rays, particularly X-rays of the δ type (Luna et al. 2013), our upper limit is still consistent with lower luminosity end of accretion-powered symbiotics.

The measured heliocentric radial velocities (see Table 2) point for a possible ionization-potential-dependent stratification in EF Aql. Similar effect is detected in the D-type symbiotic RR Tel (Kotnik-Karuza et al. 2004) and in some S-type symbiotic stars (Friedjung et al. 2010). A velocity stratification of various spectral lines is also detected in some Mira-type variables (Scholz 1992). Single Mira-type variables can usually produce many strong emission lines in their spectra (Merrill 1960; Fox, Wood & Dopita 1984), e.g. the Fe II lines. On the other hand, the broad Balmer lines and the forbidden lines of the oxygen originate from the circumbinary material.

5 CONCLUSIONS

We obtained high-resolution optical spectroscopy and X-ray observations of the D-type symbiotic star EF Aql. Using the spectra and additional photometry, we estimated the temperature ($T_{\rm hot}$ $\sim$ 55 000 K) and the luminosity ($L_{\rm hot}$ $\sim$ 5.3 $L_\odot$) of the hot component in the system. The measured parameters of the emission lines in the spectra reveal possible ionization-potential-dependent stratification. We performed periodogram analysis on the available *V*-band photometric data and found an improved period of 320.4 $\pm$ 0.3 d, which is the period of pulsations of the Mira-type donor star.

The *Swift* observation did not detect EF Aql in X-rays. The upper limit of the X-ray observations is 0.003 counts s^{-1} that, for a δ-type spectrum, corresponds into an unabsorbed flux of 10^{-12} erg cm^{-2} s^{-1}. This means that EF Aql may well be comparable to the X-ray faintest δ-type symbiotics detected so far. However, we detected EF Aql in the UV with an average *UVM2* magnitude of 14.05. Based on IR data, we estimate the distance to EF Aql to be $\sim$3.1 kpc and a mass-loss rate of the Mira donor of $\sim$2.5 $\times$ 10^{-7} $M_\odot$ yr^{-1}. The optical and X-ray observations point that EF Aql is an accretion-powered symbiotic star without shell burning. The results are proof that the D-type symbiotic stars deserve more attention and observations, which can help to understand the binary companions to AGB stars and their evolution.

ACKNOWLEDGEMENTS

We thank the anonymous referee for the comments that improved the paper. This work is supported by the grant КП-06-H28/2 08.12.2018 (Bulgarian National Science Fund). This paper is based on spectroscopic observations made with the Southern African Large Telescope (SALT) under programme 2018-1-MLT-005 (PI: J. Mikołajewska). Polish participation in SALT is funded by grant no. MNiSW DIR/WK/2016/07. This research has been partly funded by the National Science Centre, Poland, through grant OPUS 2017/27/B/ST9/01940 to JMi. GJML is a member of the CIC-CONICET (Argentina) and acknowledges support from grant ANPCYT-PICT 0901/2017. JMa acknowledges support by Agencia Estatal de Investigación grant AYA2016-76012-C3-3-P from the Spanish Ministerio de Economía y Competitividad (MINECO), and by Consejería de Economía, Innovación, Ciencia y Empleo, Junta de Andalucía under research group FQM-322, and FEDER funds.

We thank Brad Cenko, the PI of the *Neil Gehrels Swift Observatory*, for a general allocation of observing time. This research has made use of the NASA/IPAC Infrared Science Archive, which is operated by the Jet Propulsion Laboratory, California Institute of Technology, under contract with the National Aeronautics and Space Administration and the XRT Data Analysis Software (XRTDAS) developed under the responsibility of the ASI Science Data Center (ASDC), Italy. The authors acknowledge the variable star observations from the AAVSO International Database contributed by observers worldwide and used in this research. ASAS-SN is supported by the Gordon and Betty Moore Foundation through grant GBMF5490 to the Ohio State University and NSF grant AST-1515927. Development of ASAS-SN has been supported by NSF grant AST-0908816, the Mt. Cuba Astronomical Foundation, the Center for Cosmology and AstroParticle Physics, Ohio State University, the Chinese Academy of Sciences South America Center for Astronomy (CAS-SACA), the Villum Foundation, and George Skestos.

REFERENCES

Allen D. A., 1982, in Friedjung M., Viotti R., eds, The Nature of Symbiotic Stars. Reidel, Dordrecht, p. 27
Ballester P., 1992, in Grosbøl P. J., de Ruijsscher R. C. E., eds, ESO Conf. Workshop Proc. No. 41, 4th ESO/ST-ECF Data Analysis Workshop. European Southern Observatory (ESO), Garching, Germany, p. 177
Bramall D. G. et al., 2010, Proc. SPIE, 7735, 77354F
Bramall D. G. et al., 2012, Proc. SPIE, 8446, 84460A
Buckley D. A. H., Swart G. P., Meiring J. G., 2006, Proc. SPIE, 6267, 62670Z
Crause L. A. et al., 2014, Proc. SPIE, 9147, 91476T
Crawford S. M. et al., 2010, Proc. SPIE, 7737, 773725
Davidsen A., Malina R., Bowyer S., 1977, ApJ, 211, 866
Fox M. W., Wood P. R., Dopita M. A., 1984, ApJ, 286, 337
Friedjung M., Mikołajewska J., Zajczyk A., Eriksson M., 2010, A&A, 512, A80
Gromadzki M., Mikołajewska J., Whitelock P., Marang F., 2009, Acta Astron., 59, 169
Gromadzki M., Mikołajewska J., Soszyński I., 2013, Acta Astron., 63, 405
Hinkle K. H., Fekel F. C., Joyce R. R., Wood P., 2013, ApJ, 770, 28
Höfner S., Olofsson H., 2018, A&AR, 26, 1
Jura M., 1994, ApJ, 422, 102
Kalirai J. S., Marigo P., Tremblay P.-E., 2014, ApJ, 782, 17
Kniazev A. Y., Gvaramadze V. V., Berdnikov L. N., 2017, in Balega Yu. Yu., Kudryavtsev D. O., Romanyuk I. I., Yakunin I. A., eds, ASP Conf. Ser. Vol. 510, Stars: From Collapse to Collapse. Astron. Soc. Pac., San Francisco, p. 480
Kochanek C. S. et al., 2017, PASP, 129, 104502
Kotnik-Karuza D., Friedjung M., Exter K., Keenan F. P., Pollacco D. L., Whitelock P. A., 2004, in Hilditch R. W., Hensberge H., Pavlovski K., eds, ASP Conf. Ser. Vol. 318, Spectroscopically and Spatially Resolving the Components of the Close Binary Stars. Astron. Soc. Pac., San Francisco, p. 363
Kuranov A. G., Postnov K. A., 2015, Astron. Lett., 41, 114
Le Bertre T., Tanaka M., Yamamura I., Murakami H., 2003, A&A, 403, 943
Luna G. J. M., Sokoloski J. L., Mukai K., Nelson T., 2013, A&A, 559, A6
Lutz J. H., Kaler J. B., Shaw R. A., Schwarz H. E., Aspin C., 1989, PASP, 101, 966
Margon B., Prochaska J. X., Tejos N., Monroe T., 2016, PASP, 128, 024201
Merrill P. W., 1960, in Greenstein J. L, ed., Spectra of Long-Period Variables in Stellar Atmospheres. Univ. Chicago Press, Chicago, p. 509
Mikołajewska J., 2012, Balt. Astron., 21, 5
Mikolajewska J., Acker A., Stenholm B., 1997, A&A, 327, 191
Muerset U., Nussbaumer H., Schmid H. M., Vogel M., 1991, A&A, 248, 458
Munari U., Patat F., 1993, A&A, 277, 195
Munari U., Zwitter T., 1997, A&A, 318, 269
Murset U., Nussbaumer H., 1994, A&A, 282, 586
Netzer H., 1975, MNRAS, 171, 395
Neugebauer G. et al., 1984, ApJ, 278, L1
O'Donoghue D. et al., 2006, MNRAS, 372, 151
Orio M., Zezas A., Munari U., Siviero A., Tepedelenlioglu E., 2007, ApJ, 661, 1105
Paczynski B., Zytkow A. N., 1978, ApJ, 222, 604
Peterson B. M., 1997, An Introduction to Active Galactic Nuclei. Cambridge Univ. Press, Cambridge
Pojmanski G., 1997, Acta Astron., 47, 467
Reinmuth K., 1925, Astron. Nachr., 225, 385
Richwine P., Bedient J., Slater T., Mattei J. A., 2005, J. Am. Assoc. Var. Star Obser., 34, 28
Roberts D. H., Lehar J., Dreher J. W., 1987, AJ, 93, 968
Schmid H. M., 1989, A&A, 211, L31
Scholz M., 1992, A&A, 253, 203
Shappee B. et al., 2014, Am. Astron. Soc. Meeting Abstr., #223, 236.03
Sokoloski J. L., Bildsten L., Ho W. C. G., 2001, MNRAS, 326, 553
Stahl O., Kaufer A., Tubbesing S., 1999, in Guenther E., Stecklum B., Klose S., eds, ASP Conf. Ser. Vol. 188, Optical and Infrared Spectroscopy of Circumstellar Matter. Astron. Soc. Pac., San Francisco, p. 331
Stellingwerf R. F., 1978, ApJ, 224, 953
Trabucchi M., Wood P. R., Montalbán J., Marigo P., Pastorelli G., Girardi L., 2019, MNRAS, 482, 929
Vassiliadis E., Wood P. R., 1993, ApJ, 413, 641
Webster B. L., Allen D. A., 1975, MNRAS, 171, 171
Whitelock P., Menzies J., Feast M., Marang F., Carter B., Roberts G., Catchpole R., Chapman J., 1994, MNRAS, 267, 711
Whitelock P., Marang F., Feast M., 2000, MNRAS, 319, 728
Whitelock P. A., Feast M. W., van Loon J. T., Zijlstra A. A., 2003, MNRAS, 342, 86
Whitelock P. A., Feast M. W., Van Leeuwen F., 2008, MNRAS, 386, 313
Woitke P., 2006, A&A, 460, L9
Zamanov R. K. et al., 2017, Astron. Nachr., 338, 680

This paper has been typeset from a TEX/LATEX file prepared by the author.